Robust Beamforming for NOMA-Based Cellular Massive IoT With SWIPT

Qiao Qi, *Student Member, IEEE*, Xiaoming Chen, *Senior Member, IEEE*, and Derrick Wing Kwan Ng, *Senior Member, IEEE*

***Abstract*—In this paper, we study the resource allocation design for non-orthogonal multiple access (NOMA)-based cellular massive Internet-of-Things (IoT) enabled with simultaneous wireless information and power transfer (SWIPT). The design is formulated as a non-convex optimization problem, which takes into account practical and adverse factors, e.g., the channel uncertainty during channel state information (CSI) acquisition, the non-linear receiver during energy harvesting (EH) and the imperfect successive information cancellation (SIC) during the information decoding (ID). The originally harmful co-channel interference in massive access is coordinated to strike a balance between efficient information transmission and efficient energy harvesting via spatial beamforming. Subsequently, two robust beamforming algorithms are designed from the aspects of the weighted sum rate maximization and the total power consumption minimization, respectively. It is found that overall performance can be improved by adding BS antennas due to more array gains. Moreover, it is proved that the proposed algorithms can effectively alleviate the influence of adverse practical conditions and achieve the best performance compared to the baseline ones, which demonstrates the effectiveness and robustness of proposed algorithms for cellular massive IoT.**

***Index Terms*—Massive access, NOMA, cellular IoT, SWIPT, non-linear EH, imperfect SIC, robust beamforming.**

I. Introduction

THE explosive development of the Internet-of-Things (IoT) spurs a huge demand for a massive number of smart devices to access wireless networks concurrently via the same spectrum. It is predicted that more than 20.4 billion devices will connect the Internet wirelessly by 2020 [2]. In this context, the 3rd generation partnership project (3GPP) has already identified massive IoT as one of the three main use cases of the upcoming fifth generation (5 G) wireless networks, namely cellular IoT [3]. It is expected to provide seamless access over a wide range for various envisioned IoT applications, such as smart city, smart manufacturing, smart transportation, e-health care, etc [4], [5].

In most of current IoT networks, orthogonal multiple access (OMA) techniques, e.g., time division multiple access (TDMA) and frequency division multiple access (FDMA), are adopted for simplicity of transceiver design. Yet, such approaches substantially restrict the number of accessible IoT devices due to limited spectrum resource. Under the circumstances, non-orthogonal multiple access (NOMA), as a feasible massive access technique with a high spectral efficiency, has gained considerable attention at present [6]–[8]. In general, the NOMA technique employs superposition coding at the transmitter to implement massive spectrum sharing, and then makes use of successive interference cancellation (SIC) at the receivers to decrease the co-channel interference made for non-orthogonal transmission [9], [10]. However, SIC is not a trivial task in practical systems. Especially for the simple IoT devices, decoding errors occur at some SIC stages, resulting in error propagation [11], [12]. Moreover, the computational complexity of SIC is proportional to the number of access devices, which is unaffordable for the IoT devices. For reducing the SIC decoding error probability and to lessen the signal processing burden, it is usual to arrange IoT devices into several clusters, namely user clustering, and SIC is only performed within each cluster [13], [14]. Yet, inter-cluster interference does exist across the clusters, which degrades the system performance. In order to mitigate the inter-cluster interference, spatial beamforming is usually adopted at the multiple-antenna base station (BS) [15], [16]. Considering the existence of channel uncertainty in practice, in [17] and [18], robust beamforming algorithms for NOMA system were developed based on the worst-case optimization problem and the outage-constrained optimization problem, respectively.

In addition to the spectrum limitation, the energy limitation also dramatically affects the performance of cellular IoT. Currently, IoT devices are usually powered by batteries, which have limited energy power. Yet, charging or replacing batteries frequently for plenty of IoT devices incurs an exceedingly high cost. Besides, wirely charging some battery-powered IoT devices is not an easy issue in some certain scenarios, e.g., under the water or in the wall. To tackle this issue, wireless power transfer on the

Manuscript received May 30, 2019; revised October 22, 2019; accepted December 3, 2019. Date of publication December 11, 2019; date of current version December 27, 2019. The associate editor coordinating the review of this manuscript and approving it for publication was Prof. Chandra Ramabhadra Murthy. The work of X. Chen was supported in part by the National Natural Science Foundation of China under Grant 61871344, in part by the Zhejiang Provincial Natural Science Foundation of China under Grant LR20F010002, in part by the National Science and Technology Major Project of China under Grant 2018ZX03001017-002, and in part by the National Key R&D Program of China under Grant 2018YFB1801104. The work of D. W. K. Ng was supported in part by the UNSW Digital Grid Futures Institute, UNSW, Sydney, under a cross-disciplinary fund scheme and in part by the Australian Research Council's Discovery Early Career Researcher Award (DE170100137). This paper was presented in part at the IEEE/CIC International Conference on Communications in China, Changchun, China, August 2019 [1]. *(Corresponding author: Xiaoming Chen.)*

Q. Qi and X. Chen are with the College of Information Science and Electronic Engineering, Zhejiang University, Hangzhou 310027, China (e-mail: qiqiao1996@zju.edu.cn; chen_xiaoming@zju.edu.cn).

D. W. K. Ng is with the School of Electrical Engineering and Telecommunications, University of New South Wales, Sydney, NSW 2052, Australia (e-mail: w.k.ng@unsw.edu.au).

Digital Object Identifier 10.1109/TSP.2019.2959246

strength of radio frequency (RF) signals, namely wireless charging, is applied to the cellular IoT by making use of the broadcast nature of RF signals [19], [20]. A challenge of wireless power transfer is the low power transfer efficiency due to the signal carrier associated path loss and channel fading. To enhance the efficiency of wireless power transfer over fading channels, energy beamforming was proposed in [21] and [22], which exploited the CSI to focus wireless energy to particular spatial directions.

To achieve sustainable communications of a massive number of simple IoT devices over a limited radio spectrum, a feasible way is simultaneous wireless information and power transfer (SWIPT) based on NOMA with clustering. Note that NOMA with clustering leads to severe co-channel interference. On the one hand, co-channel interference decreases the quality of the information signal. On the other hand, co-channel interference increases the amount of energy harvesting. In order to improve the overall performance of cellular massive IoT with SWIPT, it is necessary to coordinate the co-channel interference by spatial beamforming. Yet, since the BS usually has partial CSI, robust beamforming has to be designed to guarantee the performance in the worst case.

A. Related Works

Robust design for SWIPT is widely regarded as a promising technique to realize sustainable communications in practical environments, and hence receives considerable interests in the past years. To this end, some preliminary works have been studied in various aspects of robust beamforming design. For example, a beamfoming algorithm for downlink SWIPT systems with imperfect CSI was investigated in [23]. The authors in [24] studied a joint robust receive and transmit beamforming design for SWIPT full-duplex MIMO system. Additionally, in [25], the authors extended the CSI error model to design robust beamforming algorithm by maximizing the weighted sum rate with a linearly precoded for a multicellular system. Moreover, since multiple-antenna beamforming can effectively improve the performance of both information transmission and energy transfer, many beamforming schemes are designed for various SWIPT scenarios. In [26], a robust beamforming for a three-node cooperative NOMA system with SWIPT was analyzed and designed. Also, the authors in [27] proposed two robust beamforming schemes for minimizing the transmit power and maximizing the harvested energy of a NOMA cognitive radio network with SWIPT, respectively.

In general, most existing works consider robust SWIPT for human-centric communications (HCC). Specifically, there are a few or even only two users in the system, where the BS broadcasts information and energy signals to the users directly. However, in the cellular IoT, there are a massive number of devices, and the existing methods proposed for a small number of devices might be not applicable. Compared with a general SWIPT system studied in the literature, the NOMA-based cellular massive IoT enabled with SWIPT experiences much severe and complicated interference, including intra-cluster interference and inter-cluster interference. Hence, it is not a trivial task to coordinate the interference by spatial beamforming. Especially, in the scenario of partial CSI, robust beamforming design for cellular massive IoT with SWIPT has not been well addressed.

B. Contributions

In this paper, we consider a sustainable cellular IoT network enabled with massive SWIPT, which is a typical application scenario of massive machine-type communications (mMTC) in 5 G and beyond. The main contributions of this paper are threefold:

1) We provide a design framework of sustainable cellular massive IoT with SWIPT. The benefits of spatial beamforming offered by the multiple-antenna BS are exploited to enhance the efficiencies of both information transformation and energy harvesting (EH) under practical conditions.
2) We consider a practical SWIPT scenario in the massive cellular IoT, where the BS only obtains partial CSI, and the simple loT device has a non-linear EH receiver and carries out imperfect SIC during information decoding (ID). In particular, we investigate the impacts of practical factors, e.g., partial CSI, imperfect SIC, and non-linear EH on the performance of cellular IoT with SWIPT.
3) We propose two robust beamforming algorithms in the sense of maximizing the weighted sum rate and minimizing the total power consumption for the cellular IoT to alleviate the impacts of the adverse factors, and show that the proposed algorithms are applicable to practical SWIPT systems with low complexity and high robustness by analysis and simulations.

C. Organization and Notations

The rest of this paper is outlined as follows: Section II gives a concise introduction of a cellular IoT network with SWIPT. Section III concentrates on the design of two robust beamforming algorithms from the aspects of the weighted sum rate maximization and the total power consumption minimization. Section IV shows several simulation results to validate the effectiveness and robustness of the proposed algorithms. Finally, Section V summarizes the whole paper.

Notations: We use bold upper (lower) letters to denote matrices (column vectors), $(\cdot)^H$ to denote conjugate transpose, $\|\cdot\|$ to denote the L_2-norm of a vector, $|\cdot|$ to denote the absolute value, $\mathrm{Re}\{\cdot\}$ to denote the real part of a complex number, $\mathrm{tr}(\cdot)$ to denote trace of a matrix, $\mathrm{Rank}(\cdot)$ to denote rank of a matrix, $\lambda(\cdot)$ to denote the eigenvalue of a matrix, $\langle\cdot,\cdot\rangle$ denotes the vector inner product, and $\mathbb{C}^{M\times N}$ to denote the set of M-by-N dimensional complex matrix.

II. System Model

Let us consider a sustainable 5 G cellular IoT network as shown in Fig. 1, where a BS equipped with N_t antennas simultaneously broadcasts information and energy to K IoT user equipments (UEs) equipped with single antenna over the same carrier. For the sake of increasing the efficiency of both information and power transfer, a multi-antenna BS adopting NOMA technique

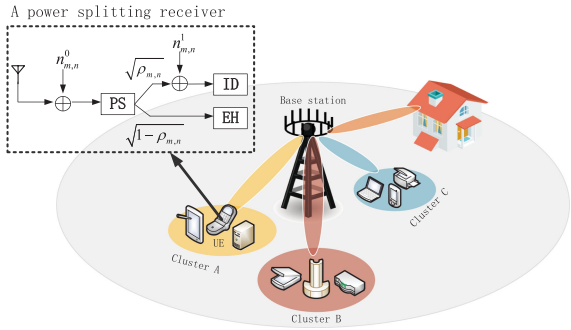

Fig. 1. A model of a cellular IoT network with SWIPT.

is considered where user clustering[1] and spatial beamforming are applied. Specifically, the BS first obtains the spatial direction of each UE through some methods, like GPS or location tracking technique. Note that in this paper, we consider a cellular massive IoT network where the UEs in general need to keep in touch with the multi-antenna BS in real time, and hence it is reasonably assumed that the BS can obtain the location of UEs. Then, the BS arranges UEs in the identical spatial direction but with distinct propagation distances into a cluster, and the UEs in the same cluster share a spatial beam. Without loss of generality, we assume that the K UEs are divided into M clusters, and the mth cluster, $\forall m \in \{1, \ldots, M\}$, contains N_m UEs. For simplicity of notation, we use $\text{UE}_{m,n}$ to represent the nth UE in the mth cluster. As shown in Fig. 1, a power splitting (PS) receiver is deployed at each UE, and thus the received RF signal at $\text{UE}_{m,n}$ is split into two components via PS with a $\rho_{m,n} : 1-\rho_{m,n}$ proportion, where $0 \le \rho_{m,n} \le 1$ is the PS ratio. The $\rho_{m,n}$ part of the received RF signal is input to the information decoding (ID) receiver and the rest $1-\rho_{m,n}$ part is sent to the energy harvesting (EH) receiver.

In this paper, it is assumed that the channels remain unchanged in a time slot, but independently fade over time slots, and partial CSI is acquired by the BS through estimation or feedback at the start of each time slot. In the light of the available CSI, the BS implements superposition coding to realize massive spectrum sharing among the K IoT UEs. Generally speaking, superposition coding includes two steps for such a massive SWIPT system, i.e., power allocation and transmit beamforming. First, the BS constructs the transmit signal x_m for the mth cluster as below:

$$x_m = \sum_{n=1}^{N_m} \sqrt{\alpha_{m,n}} s_{m,n}, \tag{1}$$

where $s_{m,n}$ denotes the Gaussian distributed signal of unit norm for the $\text{UE}_{m,n}$, and $\alpha_{m,n}$ represents the intra-cluster power allocation factor for coordinating the intra-cluster interference.

[1]Carrying out user clustering in such a SWIPT system is beneficial to achieve a balance between the system performance and computational complexity. On the one hand, for the UEs in a cluster, the identical spatial direction is conducive to boost the channel gain and to coordinate the inter-cluster interference. On the other hand, the distinctive propagation distances between the BS and UEs lessen the difficulty of the SIC at the IoT UEs.

Then, the BS constructs the total transmit signal $\mathbf{x}$ as follows:

$$\mathbf{x} = \sum_{m=1}^{M} \mathbf{w}_m x_m, \tag{2}$$

where $\mathbf{w}_m$ is an N_t-dimensional transmit beam designed for the mth cluster based on available CSI for coordinating the inter-cluster interference. Finally, the BS broadcasts the signal $\mathbf{x}$ over the downlink channels. Therefore, the received signal at the $\text{UE}_{m,n}$ can be expressed as

$$y_{m,n} = \mathbf{h}_{m,n}^H \mathbf{x} + n_{m,n}^0, \tag{3}$$

where $\mathbf{h}_{m,n}$ denotes the N_t-dimensional channel vector from the BS to the $\text{UE}_{m,n}$. In fact, each UE knows its own effective channel gain by channel estimation for coherent detection. As a result, the BS can obtain the effective channel gains conveyed by UEs through the uplink channel and line them up in each cluster. Then, the order of effective channel gains is informed to the UEs via the downlink channel. Without loss of generality, we assume that the channel gains in the mth cluster are sorted in descending order as:

$$\|\mathbf{h}_{m,1}\|^2 \ge \|\mathbf{h}_{m,2}\|^2 \ge \cdots \ge \|\mathbf{h}_{m,N_m}\|^2. \tag{4}$$

Then, based on the order of channel gains in (4), the ith UE decodes and subtracts the interfering signals linked to the N_mth to $(i+1)$th UEs at first. If SIC is carried out perfectly, the intra-cluster interference originated from the UEs with weaker channel gains can be removed entirely. However, as a matter of fact, the decoding error often occur at the weak interference signal because of the hardware restriction of the IoT UEs, the low signal quality and other factors. Thus, there exists residual interference from the weak UEs after SIC. As a rule, the residual interference resulting from imperfect SIC is an intractable function of multiple factors, e.g., coding/modulation related parameters, channel related issues (fading and shadowing), device/hardware/battery related restrictions, etc. Especially, owing to the traits of error propagation of imperfect SIC, it is hard to model the impact of imperfect SIC. Moreover, it is worth mentioning that for some certain simple IoT UEs with scanty computational capability, SIC is not a trivial task. That is to say, they do not have enough ability of carrying out SIC. In [13] and [14], a linear model is given to capture the general impacts of SIC imperfection. Under such a model, via PS, the post-SIC signal at the $\text{UE}_{m,n}$ for ID can be expressed as

$$\begin{aligned} y_{m,n}^{\text{ID}} &= \sqrt{\rho_{m,n}}(\mathbf{h}_{m,n}^H \mathbf{x} + n_{m,n}^0) + n_{m,n}^1 \\ &= \sqrt{\rho_{m,n}\alpha_{m,n}} \mathbf{h}_{m,n}^H \mathbf{w}_m s_{m,n} + \sqrt{\rho_{m,n}} n_{m,n}^0 + n_{m,n}^1 \\ &\quad + \sqrt{\rho_{m,n}} \mathbf{h}_{m,n}^H \mathbf{w}_m \sum_{i=1}^{n-1} \sqrt{\alpha_{m,i}} s_{m,i} \\ &\quad + \sqrt{\rho_{m,n}\eta_{m,n}} \mathbf{h}_{m,n}^H \mathbf{w}_m \sum_{i=n+1}^{N_m} \sqrt{\alpha_{m,i}} s_{m,i} \\ &\quad + \sqrt{\rho_{m,n}} \mathbf{h}_{m,n}^H \sum_{j=1, j\ne m}^{M} \mathbf{w}_j \sum_{i=1}^{N_j} \sqrt{\alpha_{j,i}} s_{j,i}, \end{aligned} \tag{5}$$

where $n^0_{m,n}$ denotes additive white Gaussian noise (AWGN) at the $\text{UE}_{m,n}$ with variance σ_0^2, $n^1_{m,n}$ is the baseband AWGN caused by the RF band to baseband signal conversion with variance σ_1^2, and $0 \leq \eta_{m,n} \leq 1$ represents the coefficient of imperfect SIC at the $\text{UE}_{m,n}$, which can be acquired by long-term measurement[2]. Note that $\eta_{m,n} = 0$ means perfect SIC, $0 < \eta_{m,n} < 1$ represents imperfect SIC, and $\eta_{m,n} = 1$ denotes no SIC. As a consequence, the received signal-to-interference-plus-noise ratio (SINR) at the ID receiver of $\text{UE}_{m,n}$ is given by (6) shown at the bottom of this page. In addition, the received signal at the EH receiver of $\text{UE}_{m,n}$ can be expressed as

$$y^{\text{EH}}_{m,n} = \sqrt{1-\rho_{m,n}}(\mathbf{h}^H_{m,n}\mathbf{x} + n^0_{m,n}). \tag{7}$$

According to Eq. (7), the input power at the EH receiver of $\text{UE}_{m,n}$ is given by

$$P^{\text{in}}_{m,n} = (1-\rho_{m,n})\left(\sum_{j=1}^{M}\left|\mathbf{h}^H_{m,n}\mathbf{w}_j\right|^2 + \sigma_0^2\right). \tag{8}$$

If the conventional linear EH model [28]–[30] is employed, the harvested energy at $\text{UE}_{m,n}$ can be expressed as

$$\begin{aligned} P^{(\text{L})}_{m,n} &= \vartheta_{m,n} P^{\text{in}}_{m,n} \\ &= \vartheta_{m,n}(1-\rho_{m,n})\left(\sum_{j=1}^{M}\left|\mathbf{h}^H_{m,n}\mathbf{w}_j\right|^2 + \sigma_0^2\right), \end{aligned} \tag{9}$$

where $\vartheta_{m,n} \in (0,1]$ stands for the energy conversion efficiency of the EH circuit. As seen from (9), for the traditional linear EH model, the energy conversion efficiency is irrelevant to the input power at the EH receiver. However, in practice, the EH circuit shows non-linear characteristics due to hardware restrictions such as the current leakage and circuit sensitivity limitations [31], [32]. Concretely, the harvested energy first improves as the input power increases in the low power region, but it will be saturated when the input power is sufficiently large. Obviously, the classical linear EH model is not exact especially for high received power, which may give rise to severe performance loss. Thus, we employ a more practical EH model for accurately capturing the impact of the non-linear phenomena, namely non-linear EH model [23]. Under the non-linear EH model, the harvested energy at the $\text{UE}_{m,n}$ is given by

$$P^{(\text{NL})}_{m,n} = \frac{\frac{M_{m,n}}{1+\exp(-a_{m,n}(P^{\text{in}}_{m,n}-b_{m,n}))} - \frac{M_{m,n}}{1+\exp(a_{m,n}b_{m,n})}}{1-\frac{1}{1+\exp(a_{m,n}b_{m,n})}}, \tag{10}$$

[2]Through off-line measuring a great number of samples for a long training time, based on the central limit theorem, the residual interference can be accurately approximated utilizing a Gaussian distribution, and the variance can be represented by the received power [10]. Then, the BS can obtain the imperfect SIC coefficient $\eta_{m,n}$ via comparing the powers of the residual interference and the received signal.

where $M_{m,n}, a_{m,n}$ and $b_{m,n}$ are constants related to system parameters of the EH circuit. $M_{m,n}$ denotes the maximum harvested power at the $\text{UE}_{m,n}$ with the saturated EH circuit, $a_{m,n}$ and $b_{m,n}$ are parameters in regard to the detailed circuit specification including the capacitance and resistance.

As seen in (6) and (10), the performance of both ID and EH is affected by the interference due to massive access. On the one hand, the interference decreases the quality of the received signal for ID. On the other hand, the interference increases the total amount of power of the received signal for EH. Thus, it is imperative to achieve a balance between ID and EH. Since the interference can be coordinated through transmit beamforming, optimizing the spatial beams serves as a key to improve the overall performance of the cellular IoT with SWIPT, especially under the adverse conditions of imperfect SIC and non-linear EH. Note that the optimization of spatial beams requires accurate CSI at the BS. However, in practical cellular IoT, the BS only has partial CSI. In this context, it is necessary to design robust beamforming algorithms for realizing sustainable communications of a massive number of IoT UEs.

III. Robust Design of Massive SWIPT

In this section, we design robust massive SWIPT algorithms for the cellular IoT with imperfect SIC and non-linear EH. As mentioned above, the BS obtains partial CSI through estimation or feedback, and thus there always exists channel uncertainty at the BS. In general, there are two main methods to capture the effect of channel uncertainty, which differ in the way the CSI errors are modeled, i.e., the deterministic model and the probabilistic model. Actually, the probabilistic model can be converted to the deterministic model under some mild conditions [33]. According to the characteristics of cellular IoT, we adopt a classical deterministic CSI error model with the uncertainty assumed to lie in a given ellipsoid [27], in order to obtain the effect of channel uncertainty and to separate the specific channel estimation method used from the beamforming design. In particular, the relationship between the real channel vector $\mathbf{h}_{m,n}$ and the estimated CSI $\hat{\mathbf{h}}_{m,n}$ can be expressed as

$$\mathbf{h}_{m,n} \in \mathcal{H}_{m,n} = \{\hat{\mathbf{h}}_{m,n} + \mathbf{e}_{m,n} | \, \|\mathbf{e}_{m,n}\| \leq \epsilon_{m,n}\}, \tag{11}$$

where $\mathbf{e}_{m,n}$ is the channel estimation error, the norm of which is bounded by $\epsilon_{m,n}$. According to the characteristics of the cellular IoT with SWIPT, the weighted sum rate (WSR) and the total power consumption (TPC) are two mainly concerned performance metrics. Therefore, we design the massive SWIPT algorithms from the perspectives of maximizing the WSR and minimizing the TPC, respectively.

$$\Gamma_{m,n} = \frac{\alpha_{m,n}\left|\mathbf{h}^H_{m,n}\mathbf{w}_m\right|^2}{\left|\mathbf{h}^H_{m,n}\mathbf{w}_m\right|^2 \sum_{i=1}^{n-1}\alpha_{m,i} + \eta_{m,n}\left|\mathbf{h}^H_{m,n}\mathbf{w}_m\right|^2 \sum_{i=n+1}^{N_m}\alpha_{m,i} + \sum_{j=1,j\neq m}^{M}\left|\mathbf{h}^H_{m,n}\mathbf{w}_j\right|^2 + \sigma_0^2 + \frac{\sigma_1^2}{\rho_{m,n}}} \tag{6}$$

A. The Weighted Sum Rate Maximization Design

With the above deterministic model of channel uncertainty in (11), we first design a robust algorithm for maximizing the WSR of the UEs while guaranteeing the EH requirements in the worst case. The robust design is formulated as the following optimization problem:

$$\max_{\mathbf{w}} \sum_{m=1}^{M}\sum_{n=1}^{N_m} \theta_{m,n} \min_{\mathbf{h}_{m,n}\in\mathcal{H}_{m,n}} R_{m,n}, \tag{12a}$$

$$\text{s.t.} \sum_{m=1}^{M} \|\mathbf{w}_m\|^2 \le P_{\max}, \tag{12b}$$

$$\min_{\mathbf{h}_{m,n}\in\mathcal{H}_{m,n}} P_{m,n}^{(\mathrm{NL})} \ge q_{m,n}, \tag{12c}$$

where $R_{m,n}=\log_2(1+\Gamma_{m,n})$ is the achievable rate (in bit/s) of the $\mathrm{UE}_{m,n}$ in the worst case, $\theta_{m,n}>0$ denotes the priority of $\mathrm{UE}_{m,n}$, $P_{\max}>0$ is the maximum transmit power budget at the BS, and $q_{m,n}>0$ is the required minimum amount of harvested energy, respectively. $\mathbf{w}=\{\mathbf{w}_1,\ldots,\mathbf{w}_M\}$ is the collection of spatial beams. Note that (12b) represents the maximum power allocation constraint, and constraint (12c) is the minimum requirement on the harvested energy of each UE. For convenience of expression, we define $Q_{m,n}\triangleq b_{m,n}-\frac{1}{a_{m,n}}\ln\frac{e^{a_{m,n}b_{m,n}}(M_{m,n}-q_{m,n})}{q_{m,n}e^{a_{m,n}b_{m,n}}+M_{m,n}}$, then constraint (12c) can be rewritten as

$$\min_{\mathbf{h}_{m,n}\in\mathcal{H}_{m,n}} \sum_{j=1}^{M}\left|\left(\hat{\mathbf{h}}_{m,n}+\mathbf{e}_{m,n}\right)^H\mathbf{w}_j\right|^2+\sigma_0^2 \ge \frac{Q_{m,n}}{1-\rho_{m,n}}. \tag{13}$$

It is clear that the problem (12) is not convex, thereby it is difficult to obtain the optimal solution directly. Especially, the BS only has partial CSI, which further leads to a complicated objective function. In general, a brute force approach is required to obtain the globally solution of the problem at hand. However, it will incur a prohibitively large complicated complexity. To deal with this issue, we resort to optimizing a lower bound on the objective function. To this end, we first introduce the following lemma.

Lemma 1: For two optimization problems as follow:

$$f_1(\mathbf{x}) = \max_{\|\mathbf{x}\|\le\varepsilon} \mathrm{Re}\{\mathbf{x}^H\mathbf{y}\}, \tag{14a}$$

and

$$f_2(\mathbf{x}) = \min_{\|\mathbf{x}\|\le\varepsilon} \mathrm{Re}\{\mathbf{x}^H\mathbf{y}\}, \tag{14b}$$

where variable $\mathbf{x}$ is norm-bounded with ε and $\mathbf{y}$ is a given parameter. Their solutions are given by

$$f_1\left(\frac{\varepsilon}{\|\mathbf{y}\|}\mathbf{y}\right)=\varepsilon\|\mathbf{y}\| \tag{15a}$$

and

$$f_2\left(-\frac{\varepsilon}{\|\mathbf{y}\|}\mathbf{y}\right)=-\varepsilon\|\mathbf{y}\|, \tag{15b}$$

respectively.

Proof: It is known that $-|\mathbf{x}^H\mathbf{y}|\le\mathrm{Re}\{\mathbf{x}^H\mathbf{y}\}\le|\mathbf{x}^H\mathbf{y}|$. Then, according to the Cauchy-Schwarz inequality [34], the equation $|\langle\mathbf{x},\mathbf{y}\rangle|^2\le\langle\mathbf{x},\mathbf{x}\rangle\cdot\langle\mathbf{y},\mathbf{y}\rangle$ holds true if and only if vector $\mathbf{x}$ and vector $\mathbf{y}$ are aligned, where $\langle\cdot,\cdot\rangle$ denotes the vector inner product. Thus, we have

$$\left|\mathbf{x}^H\mathbf{y}\right|\le\|\mathbf{x}\|\,\|\mathbf{y}\|\le\varepsilon\|\mathbf{y}\|, \tag{16}$$

and

$$-\varepsilon\|\mathbf{y}\|\le\mathrm{Re}\{\mathbf{x}^H\mathbf{y}\}\le\varepsilon\|\mathbf{y}\|. \tag{17}$$

In particular, the upper bound of $\mathrm{Re}\{\mathbf{x}^H\mathbf{y}\}$ is $\varepsilon\|\mathbf{y}\|$ at the point $\mathbf{x}=\frac{\varepsilon}{\|\mathbf{y}\|}\mathbf{y}$, and the lower bound of $\mathrm{Re}\{\mathbf{x}^H\mathbf{y}\}$ is $-\varepsilon\|\mathbf{y}\|$ at the point ■

Then, we deal with the term $|\mathbf{h}_{m,n}^H\mathbf{w}_m|^2$ in the objective function (12a) by utilizing Lemma 1. Specifically, we have

$$\begin{aligned}\left|\mathbf{h}_{m,n}^H\mathbf{w}_m\right|^2 &= \left(\hat{\mathbf{h}}_{m,n}+\mathbf{e}_{m,n}\right)^H\mathbf{w}_m\mathbf{w}_m^H\left(\hat{\mathbf{h}}_{m,n}+\mathbf{e}_{m,n}\right)\\ &\approx \hat{\mathbf{h}}_{m,n}^H\mathbf{w}_m\mathbf{w}_m^H\hat{\mathbf{h}}_{m,n}\\ &\quad+2\mathrm{Re}\{\mathbf{e}_{m,n}^H\mathbf{w}_m\mathbf{w}_m^H\hat{\mathbf{h}}_{m,n}\},\end{aligned} \tag{18}$$

where the second-order error term $\mathbf{e}_{m,n}^H\mathbf{w}_m\mathbf{w}_m^H\mathbf{e}_{m,n}$ is ignored due to its tiny value compared to other terms. Based on Lemma 1, we can obtain the upper bound and the lower bound of $|\mathbf{h}_{m,n}^H\mathbf{w}_m|^2$ as

$$\left|\mathbf{h}_{m,n}^H\mathbf{w}_m\right|^2\le\hat{\mathbf{h}}_{m,n}^H\mathbf{w}_m\mathbf{w}_m^H\hat{\mathbf{h}}_{m,n}+2\epsilon_{m,n}\left\|\mathbf{w}_m\mathbf{w}_m^H\hat{\mathbf{h}}_{m,n}\right\| \tag{19}$$

and

$$\left|\mathbf{h}_{m,n}^H\mathbf{w}_m\right|^2\ge\hat{\mathbf{h}}_{m,n}^H\mathbf{w}_m\mathbf{w}_m^H\hat{\mathbf{h}}_{m,n}-2\epsilon_{m,n}\left\|\mathbf{w}_m\mathbf{w}_m^H\hat{\mathbf{h}}_{m,n}\right\|, \tag{20}$$

respectively. Thus, the lower bound of the objective function in (12) can be written as (21) shown at the bottom of this page, where $\phi_{j,i}^{m,n}$ and $\varphi_{j,i}^{m,n}$ are auxiliary variables for convenience of expression, which are defined as

$$\phi_{j,i}^{m,n}=\begin{cases}\eta_{m,n}, & \text{if } j=m \text{ and } i>n\\ 0, & \text{if } j=m \text{ and } i=n\\ 1, & \text{otherwise}\end{cases} \tag{22}$$

and

$$\varphi_{j,i}^{m,n}=\begin{cases}\eta_{m,n}, & \text{if } j=m \text{ and } i>n\\ 1, & \text{otherwise}\end{cases} \tag{23}$$

$$\sum_{m=1}^{M}\sum_{n=1}^{N_m}\left(\log_2\frac{\sum_{j=1}^{M}\sum_{i=1}^{N_j}\phi_{j,i}^{m,n}\alpha_{j,i}\left(\hat{\mathbf{h}}_{m,n}^H\mathbf{w}_j\mathbf{w}_j^H\hat{\mathbf{h}}_{m,n}-2\epsilon_{m,n}\left\|\mathbf{w}_j\mathbf{w}_j^H\hat{\mathbf{h}}_{m,n}\right\|\right)+\sigma_0^2+\frac{\sigma_1^2}{\rho_{m,n}}}{\sum_{j=1}^{M}\sum_{i=1}^{N_j}\varphi_{j,i}^{m,n}\alpha_{j,i}\left(\hat{\mathbf{h}}_{m,n}^H\mathbf{w}_j\mathbf{w}_j^H\hat{\mathbf{h}}_{m,n}+2\epsilon_{m,n}\left\|\mathbf{w}_j\mathbf{w}_j^H\hat{\mathbf{h}}_{m,n}\right\|\right)+\sigma_0^2+\frac{\sigma_1^2}{\rho_{m,n}}}\right) \tag{21}$$

To make the problem more tractable, we define $\mathbf{W}_m = \mathbf{w}_m \mathbf{w}_m^H$. Thus, the EH constraint (13) can be rewritten as

$$\sum_{j=1}^{M} \left(\hat{\mathbf{h}}_{m,n}^H \mathbf{W}_j \hat{\mathbf{h}}_{m,n} - 2\epsilon_{m,n} \left\| \mathbf{W}_j \hat{\mathbf{h}}_{m,n} \right\| \right) + \sigma_0^2 \geq \frac{Q_{m,n}}{1-\rho_{m,n}}, \tag{24}$$

and the objective function can be rewritten as

$$\max_{\mathbf{W}} \log_2 \prod_{m=1}^{M} \prod_{n=1}^{N_m} \frac{\zeta_{m,n}}{\varpi_{m,n}}, \tag{25}$$

where $\zeta_{m,n} = \sum_{j=1}^{M} \sum_{i=1}^{N_j} \phi_{j,i}^{m,n} \alpha_{j,i} (\hat{\mathbf{h}}_{m,n}^H \mathbf{W}_j \hat{\mathbf{h}}_{m,n} - 2\epsilon_{m,n} \| \mathbf{W}_j \hat{\mathbf{h}}_{m,n} \|) + \sigma_0^2 + \frac{\sigma_1^2}{\rho_{m,n}}$, $\varpi_{m,n} = \sum_{j=1}^{M} \sum_{i=1}^{N_j} \varphi_{j,i}^{m,n} \alpha_{j,i} (\hat{\mathbf{h}}_{m,n}^H \mathbf{W}_j \hat{\mathbf{h}}_{m,n} + 2\epsilon_{m,n} \| \mathbf{W}_j \hat{\mathbf{h}}_{m,n} \|) + \sigma_0^2 + \frac{\sigma_1^2}{\rho_{m,n}}$, and $\mathbf{W} = \{\mathbf{W}_1, \mathbf{W}_2, \ldots, \mathbf{W}_M\}$ is the collection of new introduced matrices. In order to further deal with the non-convex objective function (25), we define

$$e^{x_{m,n}} \triangleq \zeta_{m,n} \text{ and } e^{y_{m,n}} \triangleq \varpi_{m,n}, \tag{26}$$

where $x_{m,n}$ and $y_{m,n}$ are introduced slack variables. Since the upper bound and the lower bound of $|\mathbf{h}_{m,n}^H \mathbf{x}|^2$ are both nonnegative, we have

$$e^{x_{m,n}} \geq \sigma_0^2 + \frac{\sigma_1^2}{\rho_{m,n}} \text{ and } e^{y_{m,n}} \geq \sigma_0^2 + \frac{\sigma_1^2}{\rho_{m,n}}. \tag{27}$$

Moreover, due to the constraint of transmit power at the BS, the slack variables $x_{m,n}$ and $y_{m,n}$ are finite. Substituting (26) into the objective function (25), we obtain

$$\begin{aligned} &\max_{\mathbf{W}} \log_2 \prod_{m=1}^{M} \prod_{n=1}^{N_m} \frac{\zeta_{m,n}}{\varpi_{m,n}} \\ &= \max_{\mathbf{x},\mathbf{y},\mathbf{W}} \log_2 \prod_{m=1}^{M} \prod_{n=1}^{N_m} (e^{x_{m,n}-y_{m,n}}) \\ &= \max_{\mathbf{x},\mathbf{y},\mathbf{W}} \sum_{m=1}^{M} \sum_{n=1}^{N_m} (x_{m,n} - y_{m,n}) \log_2 e, \end{aligned} \tag{28}$$

where $\boldsymbol{x} = \{x_{1,1}, \ldots, x_{M,N_m}\}$ and $\boldsymbol{y} = \{y_{1,1}, \ldots, y_{M,N_m}\}$ are the collections of slack variables. Meanwhile, dropping the rank-one constraint, i.e., $\text{Rank}(\mathbf{W}_m) = 1$, problem (12) can be reformulated as the following semi-definite programming (SDP) problem:

$$\max_{\mathbf{x},\mathbf{y},\mathbf{W}} \sum_{m=1}^{M} \sum_{n=1}^{N_m} (x_{m,n} - y_{m,n}) \log_2 e \tag{29a}$$

$$\text{s.t. } (24), (27),$$

$$\sum_{m=1}^{M} \text{tr}(\mathbf{W}_m) \leq P_{\max}, \tag{29b}$$

$$\mathbf{W}_m \succeq \mathbf{0}, \forall m, \tag{29c}$$

$$x_{m,n} \geq y_{m,n}, \tag{29d}$$

$$\zeta_{m,n} \geq e^{x_{m,n}}, \tag{29e}$$

$$\varpi_{m,n} \leq e^{y_{m,n}}. \tag{29f}$$

Although the objective function (29a) and constraint (29e) have been transformed to convex ones, the constraint (29f) is still non-convex. In order to solve this issue, a Taylor series expansion $f(x) = \sum_{n=0}^{\infty} \frac{f^{(n)}}{n!} (x - x_0)^n + R_n(x)$ is applied. Let us define (30) shown at the bottom of this page, where $\tilde{\mathbf{W}}_m$ is a feasible point of problem (29) at the last iteration. Since $e^{y_{m,n}}$ is convex, its first-order Taylor series expansion at $\tilde{y}_{m,n}$ is $e^{\tilde{y}_{m,n}} (y_{m,n} - \tilde{y}_{m,n} + 1)$. Thus, the constraint (29f) can be transformed as

$$\varpi_{m,n} \leq e^{\tilde{y}_{m,n}} \left(y_{m,n} - \tilde{y}_{m,n} + 1 \right). \tag{31}$$

Then, for a given $\tilde{\mathbf{W}}_m$, problem (29) can be rewritten as

$$\begin{aligned} \max_{\mathbf{x},\mathbf{y},\mathbf{W}} \ & \log_2 e \sum_{m=1}^{M} \sum_{n=1}^{N_m} (x_{m,n} - y_{m,n}) \\ \text{s.t. } & (24), (27), (29\text{b}) - (29\text{e}), (31). \end{aligned} \tag{32a}$$

Hence, problem (32) is a convex optimization problem which can be effectively solved by some optimization software, i.e., CVX [36]. Furthermore, by iteratively updating the fixed point $\tilde{\mathbf{W}}_m$ according to (30) and (31), we can obtain the final solutions $\mathbf{W}_m, \forall m$, once they converge. For this proposed iteration algorithm, we have the following theorem.

Theorem 1: The solutions $\{x_{m,n}, y_{m,n}, \mathbf{W}_m\}$ to the problem (32) can be converged in the iterations.

Proof: Please refer to Appendix A. ■

Note that we drop the rank-one constraint in problem (32). In order to recover the concerned spatial beam $\mathbf{w}_m$, the $\mathbf{W}_m$ should be rank-one. According to Pataki's result ([37], Theorem 2.2), an optimal solution $\mathbf{W}_m^*$ for the downlink transmit beamforming system with multiple unicast should satisfy

$$\sum_{m=1}^{M} \frac{\text{Rank}(\mathbf{W}_m^*) \left(\text{Rank}(\mathbf{W}_m^*) + 1 \right)}{2} \leq M. \tag{33}$$

Since all the optimal solution $\mathbf{W}_m^* \neq \mathbf{0}$, we have $\text{Rank}(\mathbf{W}_m^*) \geq 1$. Combine with (33), it is easy to obtain $\text{Rank}(\mathbf{W}_m^*) = 1$, which means that the semi-definite relaxation (SDR) technique, i.e., dropping the rank-one constraint employed in problem (32), is tight. Therefore, we can obtain the unique solution $\mathbf{w}_m^*$ to problem (32) by eigenvalue decomposition (EVD) on $\mathbf{W}_m^*$, namely

$$\mathbf{w}_m^* = \sqrt{\lambda_{\max}(\mathbf{W}_m^*)} \mathbf{v}_{m,\max}^*, \tag{34}$$

$$\tilde{y}_{m,n} \triangleq \ln \left(\sum_{j=1}^{M} \sum_{i=1}^{N_j} \varphi_{j,i}^{m,n} \alpha_{j,i} \left(\hat{\mathbf{h}}_{m,n}^H \tilde{\mathbf{W}}_j \hat{\mathbf{h}}_{m,n} + 2\epsilon_{m,n} \left\| \tilde{\mathbf{W}}_j \hat{\mathbf{h}}_{m,n} \right\| \right) + \sigma_0^2 + \frac{\sigma_1^2}{\rho_{m,n}} \right) \tag{30}$$

Algorithm 1: Robust Beamforming Design for Maximizing the WSR.

Input: $\theta_{m,n}, \eta_{m,n}, \alpha_{m,n}, \rho_{m,n}, q_{m,n}, \sigma_0^2, \sigma_1^2, \epsilon_{m,n}, P_{\max}$.
Output: $\mathbf{w}_m$.

1: **Initialize** $\mathbf{w}_m^{(0)} = \sqrt{\frac{P_{\max}}{M}}[1, 0, \ldots, 0]^{\mathrm{T}}, \forall m$, the convergence accuracy Δ, the iteration index $t = 1$, the WSR $R^{(0)} = 0$, and the feasible point $\tilde{\mathbf{W}}_m^{(0)} = \mathbf{w}_m^{(0)}(\mathbf{w}_m^{(0)})^H$;
2: **while** $\Delta > 0.01$ **do**
3: Solve the convex problem (32) by CVX and get the optimal solution $\mathbf{W}_m^*$;
4: Update $\tilde{\mathbf{W}}_m^{(t)} = \mathbf{W}_m^*$, $\Delta = R^{(t)} - R^{(t-1)}$;
5: Update $t = t + 1$;
6: **end while**
7: Obtain $\mathbf{w}_m^*$ by EVD on $\mathbf{W}_m^*$ according to (34).

where $\lambda_{\max}(\mathbf{W}_m^*)$ is the maximum eigenvalue of $\mathbf{W}_m^*$, and $\mathbf{v}_{m,\max}^*$ is the unit eigenvector with respect to $\lambda_{\max}(\mathbf{W}_m^*)$. In addition, for the first-order Taylor series expansion of $e^{y_{m,n}}$ at point $\tilde{y}_{m,n}$ in constraint (29f), the closer the expansion point $\tilde{y}_{m,n}$ is to the variable $y_{m,n}$, the smaller the approximation error is. Hence, in order to set feasible initial values $\tilde{y}_{m,n}^{(0)}$ to accelerate the convergence of algorithm, we make $\tilde{\mathbf{w}}_m^{(0)} = \sqrt{\frac{P_{\max}}{M}}[1, 0, \ldots, 0]^T$ to satisfy the transmission power constraint. Accordingly, the initial value of $\tilde{y}_{m,n}^{(0)}$ is computed by (30). In summary, a robust beamforming design with massive SWIPT for maximizing the WSR can be described as Algorithm 1.

Remark 1: To explicitly show the impact of the capacity of IoT UEs on the performance of the proposed algorithm, we use the parameters $\phi_{j,i}^{m,n}$ and $\varphi_{j,i}^{m,n}$ to show the impact of imperfect SIC, i.e., $\phi_{j,i}^{m,n} = \psi_{j,i}^{m,n} = \eta_{m,n}, \forall j = m$ and $i > n$. Specifically, $\eta_{m,n} = 1$ represents that the IoT UE has no capability to perform SIC, $\eta_{m,n} = 0$ represents the ideal situation of perfect SIC, and if the IoT UE performs SIC but SIC is imperfect, $\eta_{m,n}$ is within the range (0,1). In addition, if the channel estimation error bound $\epsilon_{m,n} = 0$, it becomes the case of full CSI. Therefore, Algorithm 1 provides a general design method for massive SWIPT in cellular IoT.

B. The Total Power Consumption Minimization Design

In this section, we design a robust massive SWIPT algorithm for the cellular IoT network with the goal of minimizing the TPC at the BS, while guaranteeing QoS requirements. It is worth pointing out that although the IoT applications may have different QoS requirements, e.g., the delay, throughput and reliability, they all can be represented as a function of SINR. Thereby, the optimization problem related to the minimization of the total power consumption can be mathematically expressed as (35) shown at the bottom of this page, where $\gamma_{m,n} > 0$ is the prescribed SINR target for $\mathrm{UE}_{m,n}$, $\mathbf{w} = \{\mathbf{w}_1, \ldots, \mathbf{w}_M\}$ is the collection of spatial beams. It is seen that problem (35) is not convex due to infinitely many quadratic inequalities for SINR and EH constraints. To make problem (35) computationally tractable, we first utilize new matrix variables $\mathbf{W}_m = \mathbf{w}_m\mathbf{w}_m^H$ and introduce two useful lemmas as follows:

Lemma 2: (S-procedure, [35]) Let us consider a function $\mathbf{f}_m(\mathbf{x})$ as

$$\mathbf{f}_m(\mathbf{x}) = \mathbf{x}^H\mathbf{A}_m\mathbf{x} + 2\,\mathrm{Re}\left\{\mathbf{b}_m^H\mathbf{x}\right\} + \mathbf{c}_m, m \in \{1, 2\}, \quad \mathbf{x} \in \mathbb{C}^{N\times 1}, \tag{36}$$

where $\mathbf{A}_m \in \mathbb{C}^{N\times N}$, $\mathbf{b}_m \in \mathbb{C}^{N\times 1}$ and $\mathbf{c}_m \in \mathbb{C}^{N\times 1}$. The derivation $\mathbf{f}_1(\mathbf{x}) \le 0 \Rightarrow \mathbf{f}_2(\mathbf{x}) \le 0$ holds true if and only if there exists $\tau \ge 0$, such that

$$\tau\begin{bmatrix}\mathbf{A}_1 & \mathbf{b}_1\\ \mathbf{b}_1^H & \mathbf{c}_1\end{bmatrix} - \begin{bmatrix}\mathbf{A}_2 & \mathbf{b}_2\\ \mathbf{b}_2^H & \mathbf{c}_2\end{bmatrix} \succeq \mathbf{0}. \tag{37}$$

Lemma 3: (Schur's complement, [35]) Let $\mathbf{Y} = \left[\begin{smallmatrix}\mathbf{A} & \mathbf{B}^H\\ \mathbf{B} & \mathbf{C}\end{smallmatrix}\right]$ be a Hermitian matrix. Then $\mathbf{Y} \succeq \mathbf{0}$ holds true if and only if $\mathbf{A} - \mathbf{B}^H\mathbf{C}^{-1}\mathbf{B} \succeq \mathbf{0}$ with assuming $\mathbf{C}$ is invertible, or $\mathbf{C} - \mathbf{B}^H\mathbf{A}^{-1}\mathbf{B} \succeq \mathbf{0}$ with assuming $\mathbf{A}$ is invertible.

Now, we deal with the SINR and EH constraints based on above two lemmas. For the SINR constraint of the $\mathrm{UE}_{m,n}$, it can be further expressed as (38) shown at the bottom of this page. Let $\mathbf{Y}_{m,n} = \frac{1}{\gamma_{m,n}}\mathbf{W}_m - \sum_{j=1}^{M}\sum_{i=1}^{N_j}\phi_{j,i}^{m,n}\alpha_{j,i}\mathbf{W}_j$, the inequality (38) can be rewritten as

$$\left(\hat{\mathbf{h}}_{m,n} + \mathbf{e}_{m,n}\right)^H\mathbf{Y}_{m,n}\left(\hat{\mathbf{h}}_{m,n} + \mathbf{e}_{m,n}\right) - \sigma_0^2 - \frac{\sigma_1^2}{\rho_{m,n}} \ge 0, \tag{39}$$

$$\min_{\mathbf{w}} \sum_{m=1}^{M}\|\mathbf{w}_m\|^2 \tag{35a}$$

$$\text{s.t.} \min_{\mathbf{h}_{m,n}\in\mathcal{H}_{m,n}} \frac{\alpha_{m,n}\left|\mathbf{h}_{m,n}^H\mathbf{w}_m\right|^2}{\sum_{j=1}^{M}\sum_{i=1}^{N_j}\phi_{j,i}^{m,n}\alpha_{j,i}\left|\mathbf{h}_{m,n}^H\mathbf{w}_j\right|^2 + \sigma_0^2 + \frac{\sigma_1^2}{\rho_{m,n}}} \ge \gamma_{m,n} \tag{35b}$$

$$\min_{\mathbf{h}_{m,n}\in\mathcal{H}_{m,n}} \sum_{j=1}^{M}\left|\mathbf{h}_{m,n}^H\mathbf{w}_j\right|^2 + \sigma_0^2 \ge \frac{Q_{m,n}}{1-\rho_{m,n}} \tag{35c}$$

$$\rho_{m,n}\left[\left(\hat{\mathbf{h}}_{m,n} + \mathbf{e}_{m,n}\right)^H\left(\frac{1}{\gamma_{m,n}}\mathbf{W}_m - \sum_{j=1}^{M}\sum_{i=1}^{N_j}\phi_{j,i}^{m,n}\alpha_{j,i}\mathbf{W}_j\right)\left(\hat{\mathbf{h}}_{m,n} + \mathbf{e}_{m,n}\right) - \sigma_0^2\right] \ge \sigma_1^2 \tag{38}$$

which is equivalent to the following inequality

$$\mathbf{e}_{m,n}^H \mathbf{Y}_{m,n} \mathbf{e}_{m,n} + 2\,\mathrm{Re}\left\{\hat{\mathbf{h}}_{m,n}^H \mathbf{Y}_{m,n} \mathbf{e}_{m,n}\right\} + \hat{\mathbf{h}}_{m,n}^H \mathbf{Y}_{m,n} \hat{\mathbf{h}}_{m,n} - \left(\sigma_0^2 + \frac{\sigma_1^2}{\rho_{m,n}}\right) \geq 0. \quad (40)$$

Applying Lemma 2 and Lemma 3, and setting $\mathbf{x} = \mathbf{e}_{m,n}$ and $\tau = \beta_{m,n}$, we have (41) shown at the bottom of this page. Thus, the UE$_{m,n}$'s SINR constraint (35b) can be transformed as a linear matrix inequality (LMI) constraint, i.e.,

$$\mathbf{A}_{m,n} = \begin{bmatrix} \beta_{m,n}\mathbf{I} + \mathbf{Y}_{m,n} & \mathbf{Y}_{m,n}\hat{\mathbf{h}}_{m,n} \\ \hat{\mathbf{h}}_{m,n}^H \mathbf{Y}_{m,n}^H & \hat{\mathbf{h}}_{m,n}^H \mathbf{Y}_{m,n} \hat{\mathbf{h}}_{m,n} + \nu_{m,n} \end{bmatrix} \succeq \mathbf{0}, \quad (42)$$

where $\nu_{m,n} = -\beta_{m,n}\epsilon_{m,n}^2 - \sigma_0^2 - \frac{\sigma_1^2}{\rho_{m,n}}$. Similarly, we can obtain an equivalent form of the EH constraint (35c) as

$$\mathbf{B}_{m,n} = \begin{bmatrix} \mu_{m,n}\mathbf{I} + \mathbf{T} & \mathbf{T}\hat{\mathbf{h}}_{m,n} \\ \hat{\mathbf{h}}_{m,n}^H \mathbf{T}^H & \hat{\mathbf{h}}_{m,n}^H \mathbf{T} \hat{\mathbf{h}}_{m,n} + \varsigma_{m,n} \end{bmatrix} \succeq \mathbf{0}, \quad (43)$$

where $\mathbf{T} = \sum_{j=1}^M \mathbf{W}_j$ and $\varsigma_{m,n} = -\mu_{m,n}\epsilon_{m,n}^2 + \sigma_0^2 - \frac{Q_{m,n}}{1-\rho_{m,n}}$. Hence, we can reformulate problem (35) with transformed SINR constraint (42) and EH constraint (43) as

$$\min_{\mathbf{W},\boldsymbol{\beta},\boldsymbol{\mu}} \sum_{m=1}^M \mathrm{tr}\left(\mathbf{W}_m\right) \quad (44a)$$

$$\text{s.t. } (42), (43),$$

$$\beta_{m,n} \geq 0, \mu_{m,n} \geq 0, \quad (44b)$$

$$\mathbf{W}_m \succeq \mathbf{0}, \quad (44c)$$

$$\mathrm{Rank}(\mathbf{W}_m) = 1, \quad (44d)$$

where $\boldsymbol{\beta} = \{\beta_{1,1}, \ldots, \beta_{M,N}\}$ and $\boldsymbol{\mu} = \{\mu_{1,1}, \ldots, \mu_{M,N}\}$ are the collections of above LMIs' auxiliary coefficients, respectively. It is obvious that if we adopt a general SDR technique, i.e., dropping the rank-one constraint (44d), the problem (44) is convex and can be efficiently solved via an off-the-shelf optimization tool, e.g., CVX. However, the solution $\mathbf{W}_m$ obtained by the SDR technique is not always rank-one. In this case, we utilize an alternative method based on a penalty function to guarantee $\mathbf{W}_m$ is rank-one [35]. Since $\mathbf{W}_m$ is positive semi-definite according to (44c), all the eigenvalues of $\mathbf{W}_m$ are non-negative, i.e., $\lambda_i(\mathbf{W}_m) \geq 0, \forall m, i = 1, 2, \ldots, N_t$. Due to the fact that $\mathrm{tr}(\mathbf{W}_m) = \sum_{i=1}^{N_t} \lambda_i(\mathbf{W}_m)$, we have $\mathrm{tr}(\mathbf{W}_m) \geq \lambda_{\max}(\mathbf{W}_m)$, where $\lambda_{\max}(\cdot)$ denotes the maximum eigenvalue of a matrix. Thus, for a positive semi-definite matrix $\mathbf{W}_m$ with the constraint of $\mathrm{tr}(\mathbf{W}_m) = \lambda_{\max}(\mathbf{W}_m)$, it is easy to derive $\mathrm{Rank}(\mathbf{W}_m) = 1$. In other words, the rank-one constraint (44d) can be rewritten as

$$\mathrm{tr}(\mathbf{W}_m) - \lambda_{\max}(\mathbf{W}_m) = 0, \forall m. \quad (45)$$

Inspired by (45), we argument the difference of $\mathrm{tr}(\mathbf{W}_m)$ and $\lambda_{\max}(\mathbf{W}_m)$ to the objective function as the penalty function. Through minimizing the penalty function, it is likely to fulfill the rank-one condition in (45). Hence, the new objective function of problem (44) can be expressed as

$$\min_{\mathbf{W},\boldsymbol{\beta},\boldsymbol{\mu}} \sum_{m=1}^M \mathrm{tr}(\mathbf{W}_m) + \kappa \sum_{m=1}^M \left(\mathrm{tr}(\mathbf{W}_m) - \lambda_{\max}(\mathbf{W}_m)\right), \quad (46)$$

where $\kappa > 0$ is the penalty factor. However, the introduction of the penalty function leads to a non-convex objective function. To obtain a tractable solution, we adopt an iterative method to transform it into a convex one. Specifically, for the feasible point $\mathbf{W}_m^{(t)}$ at the tth iteration, we have

$$\mathrm{tr}\left(\mathbf{W}_m^{(t+1)}\right) - \left(\mathbf{v}_{m,\max}^{(t)}\right)^H \mathbf{W}_m^{(t+1)} \mathbf{v}_{m,\max}^{(t)} \geq \mathrm{tr}\left(\mathbf{W}_m^{(t+1)}\right) - \lambda_{\max}\left(\mathbf{W}_m^{(t+1)}\right) \geq 0, \quad (47)$$

where $\mathbf{v}_{m,\max}$ is the unit eigenvector with respect to the maximum eigenvalue $\lambda_{\max}(\mathbf{W}_m)$. Thus, the problem (44) at $(t+1)$th iteration is given by (48) shown at the bottom of this page. Note that problem (48) is convex, and thus can be solved directly. Since the penalty factor $\kappa^{(t+1)} = c\kappa^{(t)} (c > 1)$ increases during the iterations, the value of the penalty function is correspondingly decreasing. Moreover, the penalty function has a lower bound according to (47). Therefore, through iteratively updating the penalty factor κ, the objective function can be converged. Once the iteration converges, namely when $\mathrm{tr}(\mathbf{W}_m)$ is approximately equal to $\lambda_{\max}(\mathbf{W}_m)$, we have

$$\mathbf{W}_m \approx \lambda_{\max}(\mathbf{W}_m) \mathbf{v}_{m,\max} \mathbf{v}_{m,\max}^H, \quad (49)$$

Accordingly, the approximate solution to the original problem (35) can be obtained as

$$\mathbf{w}_m^* = \sqrt{\lambda_{\max}(\mathbf{W}_m)} \mathbf{v}_{m,\max}. \quad (50)$$

In summary, the proposed penalty function-based iterative method can be described as Algorithm 2.

Remark 2: For TPC minimization, the iterative algorithm is generated by finding the minimum point of the penalty function.

$$\begin{bmatrix} -\mathbf{Y}_{m,n} & -\mathbf{Y}_{m,n}\hat{\mathbf{h}}_{m,n} \\ -\hat{\mathbf{h}}_{m,n}^H \mathbf{Y}_{m,n}^H & \left(\sigma_0^2 + \frac{\sigma_1^2}{\rho_{m,n}}\right) - \hat{\mathbf{h}}_{m,n}^H \mathbf{Y}_{m,n} \hat{\mathbf{h}}_{m,n} \end{bmatrix} \preceq \beta_{m,n} \begin{bmatrix} \mathbf{I} & \mathbf{0} \\ \mathbf{0} & -\epsilon_{m,n}^2 \end{bmatrix} \quad (41)$$

$$\min_{\mathbf{W},\boldsymbol{\mu},\boldsymbol{\beta}} \sum_{m=1}^M \mathrm{tr}(\mathbf{W}_m^{(t+1)}) + \kappa^{(t+1)} \sum_{m=1}^M \left(\mathrm{tr}(\mathbf{W}_m^{(t+1)}) - \left(\mathbf{v}_{m,\max}^{(t)}\right)^H \mathbf{W}_m^{(t+1)} \mathbf{v}_{m,\max}^{(t)}\right)$$

$$\text{s.t. } (42), (43), (44\text{b}), (44\text{c}) \quad (48)$$

Algorithm 2: Robust Beamforming Design for Minimizing the TPC.

Input:
$a_{m,n}, b_{m,n}, M_{m,n}, \eta_{m,n}, \alpha_{m,n}, \rho_{m,n}, \sigma_0^2, \sigma_1^2, q_{m,n}, \gamma_{m,n}$
Output: $\mathbf{w}_m$

1: **Initialize** $\mathbf{w}_m^{(0)} = \sqrt{\frac{P_{\max}}{M}}[1, 0, \ldots, 0]^{\mathrm{T}}$, $\mathbf{W}_m^{(0)} = \mathbf{w}_m^{(0)}(\mathbf{w}_m^{(0)})^H$, a proper penalty factor κ, a proper coefficient $c > 1$, the convergence accuracy $\Delta = 10^{-12}$, the maximum number of iteration $T_{\max} = 30$ and the iteration number $t = 1$.
2: **repeat**
3: Solve problem (44) with CVX, then obtain $\mathbf{W}_m^{(t)}$.
4: **if** $\mathbf{W}_m^{(t)}$ converges **then**
5: **if** $\sum_{m=1}^{M} \mid \mathrm{tr}(\mathbf{W}_m^{(t)}) - \lambda_{\max}(\mathbf{W}_m^{(t)}) \mid > \Delta$ **then**
6: increase the penalty factor with $\kappa^{(t+1)} = c\kappa^{(t)}$.
7: **end if**
8: **end if**
9: Update $t = t + 1$.
10: **until** converges or $t > T_{\max}$.
11: Obtain $\mathbf{w}_m^*$ according to (50).

Since the value of the penalty term is forced to gradually decrease as the penalty factor increases, it is plausible to set a big initial value of penalty factor for reducing the iterations. However, a too large penalty factor makes it difficult to solve the transformed problem or even lead to an unsolvable problem, while a too small penalty factor results in more iterations. Hence, it is important to select a suitable penalty factor for Algorithm 2 [40].

C. Optimality Analysis of the Proposed Algorithms

In this section, we focus on the optimality analysis of the two proposed robust design algorithms. For the WSR maximization design, we resort to some approximation methods, i.e., Cauchy-Schwartz inequality, Taylor series expansion and SDR technique, to transform the original problem into a convex problem. Thus, the obtained solutions might be not optimal. But, the approximations will not shrink the feasible region too much over the original problem in the case that the value of uncertainty region $\epsilon_{m,n}$ is small, the step that updating the Taylor expansion point to approach the constraint (29f) in the iterations, and the fact that SDR technique is tight. Hence, it is easy to be verified that the solution we obtain during the iterations ensures the satisfaction of its original problem. For the TCP minimization design, we adopt the SDR technique to overcome the non-convexity issues in the original problem. To guarantee the rank-one constraint, an iterative function based on a penalty function is proposed. Specifically, a new objective function is constructed with the penalty function according to the rank-one constraint. The optimal solution of the primal constrained problem is gradually approached by finding the minimum point of the new objective function through a series of penalty factors. In fact, the value of the penalty term is forced to gradually decrease as the penalty factor increases. Thus, when the penalty factors go to infinity, the minimum point of the new objective function is the optimal solution of the original problem.

D. Complexity Analysis of the Proposed Algorithms

In this section, we analyze the computational complexity of the two proposed robust design algorithms. It is obvious that problems (32) and (48) are standard SDP problems, only involving LMI, second-order cone (SOC) and affine constraints, which can be effectively solved by using the interior-point method (IPM). According to the computational complexity analysis of a generic IPM for solving the SDP problem in the *Lecture* 6 of [38], for a given $\varepsilon > 0$, the computational cost for an ε-optimal solution is in the order of $\ln(1/\varepsilon)\delta$, where δ is the barrier parameter measuring the geometric complexity of the conic constraints. For simplicity of analysis of barrier parameter δ, we assume that the decision variables n in problems (32) and (48) are real-valued. First, for the problem (32), it has $2M$ LMI constraints of size N_t, $M + 2K$ SOC constraints of size N_t, and $3K$ affine constraints. Second, problem (48) has $2K$ LMI constraints of size $N_t + 1$, M LMI constraints of size N_t, and $2K$ affine constraints. Moreover, the number of decision variables n is on the order of KN_t^2. Based on the above analysis, the per-iteration complexities for our proposed algorithms are shown in Table I. In addition, to visualize the complexity, we present the computing time for per-iteration of Algorithm 1 and Algorithm 2 as the numbers of UEs and BS antennas increase, which is solved by CVX at the SDPT3 solver in the Windows 7 operating system, cf. Fig. 2, where $N_m = N = 4, \eta_{m,n} = \eta = 0.05, \epsilon_{m,n} = \epsilon = 0.1, q_{m,n} = q_0 = 10$ mW, $\gamma_{m,n} = \gamma_0 = 0.2$ dB. It is seen that compared to the exhaustive search, the proposed algorithms have low computational complexity. Hence, they are appealing in the cellular IoT with massive access.

IV. Numerical Results

This section provides some numerical results to validate the robustness and effectiveness of the proposed algorithms for massive SWIPT in the cellular IoT. Unless otherwise stated, we set $N_t = 24, K = 16, M = 4, N_m = N = 4, \eta_{m,n} = \eta = 0.05, \sigma_0^2 = 0.1, \sigma_1^2 = 1, \epsilon_{m,n} = \epsilon = 0.1, \alpha_{m,n} = n/\sum_{i=1}^{N_m} i, \rho_{m,n} = 0.8$ and $\theta_{m,n} = 1, \forall m, n$. In addition, we use SNR (in dB) to denote the ratio of transmit power at the BS and the noise variance. For the non-linear EH model, we set $M_{m,n} = 24$ mW, $a_{m,n} = 150$ and $b_{m,n} = 0.014$ according to the practical circuit parameters provided by [23]. Without loss of generality, all IoT UEs have the same required EH threshold $q_{m,n} = q_0 = 10$ mW and the same required SINR threshold $\gamma_{m,n} = \gamma_0 = 0.2$ dB.

First, we examine the convergence behaviors of the proposed Algorithm 1 under different SNR values in Fig. 3. It is seen that Algorithm 1 has a quick convergence at lower SNR, while it requires a little more number of iterations as SNR increases. In general, Algorithm 1 converges no more than 10 iterations on

TABLE I
COMPUTATION COMPLEXITY ANALYSIS OF PROPOSED ALGORITHMS

Algorithms	Complexity is in order of $\ln(1/\varepsilon)\,\delta$, where $n = \mathcal{O}(KN_t^2)$)
Algorithm 1	$\delta = \sqrt{(3M+2K)N_t + 3K} \cdot n \cdot \left[(3M+2K)\,N_t^3 + 3K + n\,(3M+2K)\,N_t^2 + 3Kn + n^2\right]$
Algorithm 2	$\delta = \sqrt{(M+2K)N_t + 4K} \cdot n \cdot \left[2K(N_t+1)^3 + MN_t^3 + 2K + (2K+M)N_t^2 + 2nKN_t + 4Kn + n^2\right]$

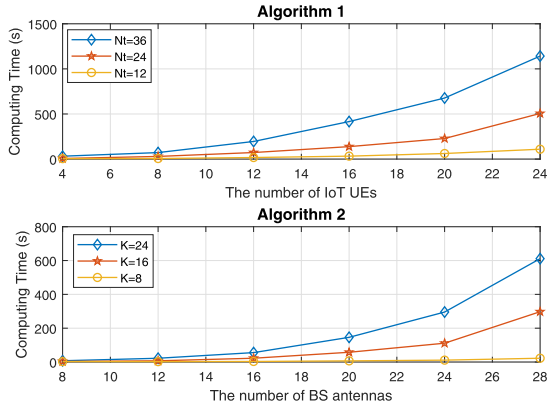

Fig. 2. Computing time for per-iteration of Algorithm 1 and Algorithm 2.

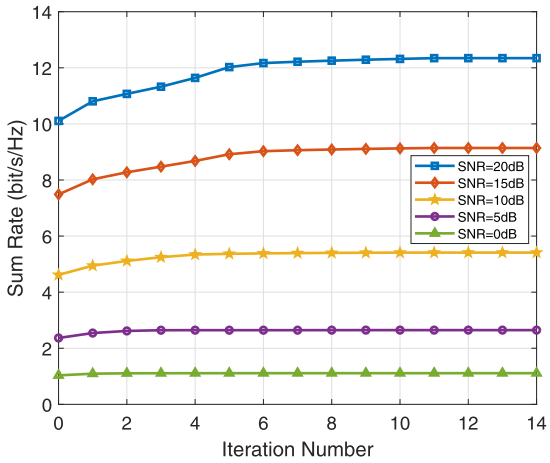

Fig. 3. Convergence behavior of the proposed Algorithm 1.

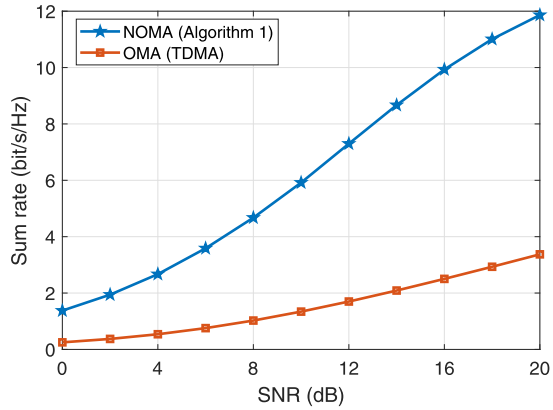

Fig. 4. Performance comparison between NOMA scheme and OMA scheme.

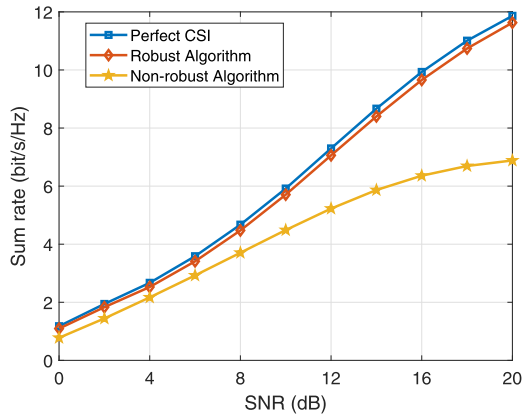

Fig. 5. Sum rate versus SNR (dB) for different beamforming design algorithms.

average under different SNR values, which means that the complexity of Algorithm 1 is affordable due to a low computational cost of per-iteration as shown in Table I.

Fig. 4 compares the sum rate performance of the proposed NOMA scheme and the conventional OMA scheme, i.e., TDMA. It is intuitive that the proposed Algorithm 1 has a significant performance gain over the TDMA. This is because compared to TDMA, the proposed Algorithm 1 effectively takes advantage of spatial multiplexing provided by the BS with a multiple-antenna array, and thus can substantially improve the performance.

Then, we illustrate the performance gain of the proposed Algorithm 1 over the non-robust algorithm (Zero-forcing beamforming) in Fig. 5. Note that the case of perfect CSI means that perfect CSI is available for beamforming design, which can achieve the performance upper bound of massive SWIPT in the cellular IoT. It is seen that Algorithm 1 taking into account the norm-bounded channel estimation error is superior to the non-robust one. In particular, the performance gap between Algorithm 1 and the non-robust algorithm increases as SNR increases. In addition, the performance loss of Algorithm 1 over the perfect CSI case is quite small, which means that Algorithm 1 is effective and robust.

Fig. 6 shows the performance of Algorithm 1 with different channel estimation error bounds. Note that the case of $\epsilon = 0$ means perfect CSI at the BS. It is found that the sum rate decreases as the channel estimation error bound increases. This is because for a given power budget, a large channel estimation error bound requires a higher transmit power to guarantee the worse case of performance and accordingly less power contributes to improving the overall performance. Moreover, the performance loss of Algorithm 1 with respect to the perfect CSI case grows with the increase of SNR, which means that ϵ has a critical impact on the sum rate at high SNR. However, the performance loss due to channel uncertainty is very limited even with $\epsilon = 0.25$, which reconfirms the robustness of Algorithm 1.

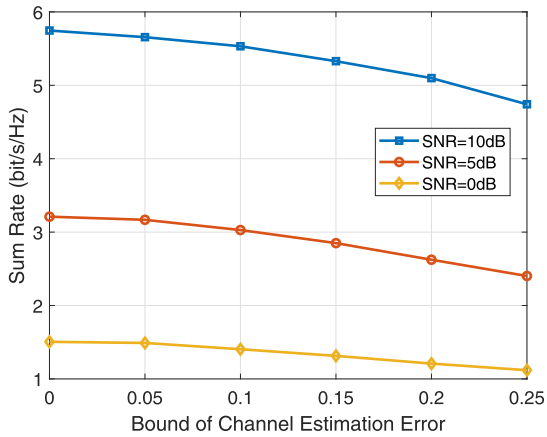

Fig. 6. Sum rate versus channel estimation error bound ϵ for different SNR (dB).

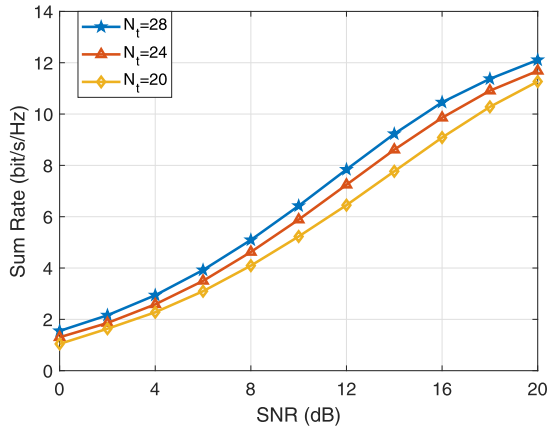

Fig. 8. Impact of the number of BS antennas N_t on the performance of Algorithm 1.

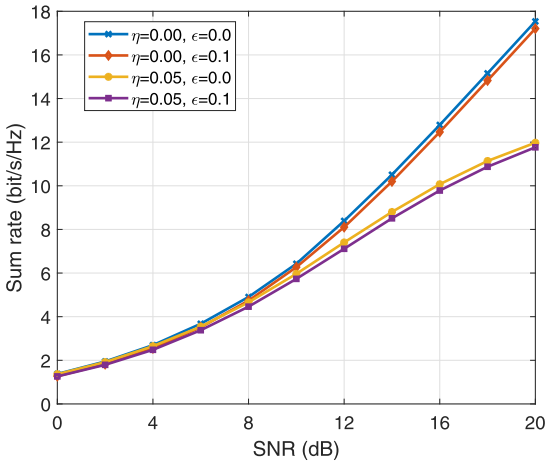

Fig. 7. Effects of imperfect SIC and partial CSI on the performance of Algorithm 1.

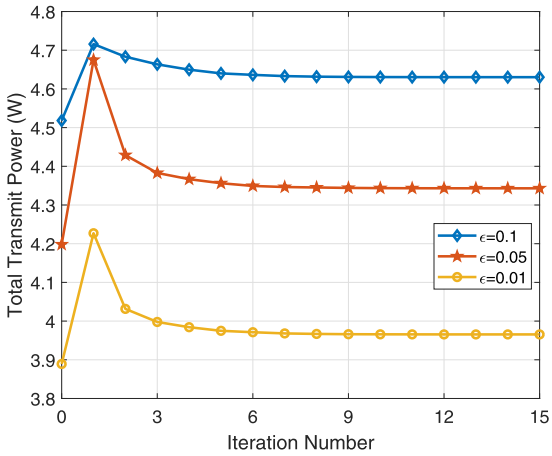

Fig. 9. Convergence behavior of the proposed Algorithm 2.

Fig. 7 investigates the capability of Algorithm 1 for alleviating the impact of imperfect SIC. It is seen that the performance loss due to imperfect SIC is slight at lower SNR, which means Algorithm 1 has a strong capability for alleviating the impact of imperfect SIC in the low SNR region. However, with the increase of SNR, the performance gap with respect to the perfect SIC case ($\eta = 0$) becomes large. This is because in the case of perfect SIC, the intra-cluster interference can be eliminated and the sum rate increases as SNR increases, while the sum rate with imperfect SIC ($\eta = 0.05$) will be quickly saturated in the high SNR region. Moreover, it is found that the performance of Algorithm 1 is quite close to that of the perfect CSI case. Thus, Algorithm 1 can address the practical issues in the cellular IoT.

In Fig. 8, we examine the impact of the number of BS antennas N_t on the sum rate of Algorithm 1. As expected, the sum rate improves as the number of BS antennas increases, because a large number of BS antennas can provide more array gains to improve the performance. Moreover, since the system is interference limited at high SNR, the sum rate is asymptotically saturated as the SNR increases. Therefore, it is possible to further improve the performance at high SNR by increasing the number of BS antennas.

Next, we show the convergence behaviors of Algorithm 2 under different channel estimation error bounds in Fig. 9. Intuitively, after the first iteration, system finds a better point as its initial point. Similar to Algorithm 1, Algorithm 2 under different conditions converges after no more than 10 times iterations as long as we set a feasible penalty factor. Moreover, it is found that a large channel estimation error bound always consumes more transmit power, which does correspond with the result in Fig. 6.

In Fig. 10, we reveal the relationship between the total power consumption and the required minimum SINR γ_0 for different channel estimation error bounds ϵ. It is observed that extra transmit power is consumed when channel estimation error is involved due to the performance compensation. Further, the total transmit power is sensitive to the channel estimation error bound and increases along with it especially at high SINR threshold. For instance, all curves almost overlap when the SINR threshold γ_0 is below 0.2 dB, but the gaps between curves grow larger as the minimum required SINR increases.

Finally, we check the impact of imperfect SIC on the power consumption of Algorithm 2 at different EH thresholds with a channel estimation error bound $\epsilon = 0.05$. From Fig. 11, it is seen that Algorithm 2 with the EH threshold $q_0 = 20$ mW consumes more transmit power than that with the EH threshold $q_0 = 10$ mW. In addition, the case of imperfect SIC ($\eta = 0.05$)

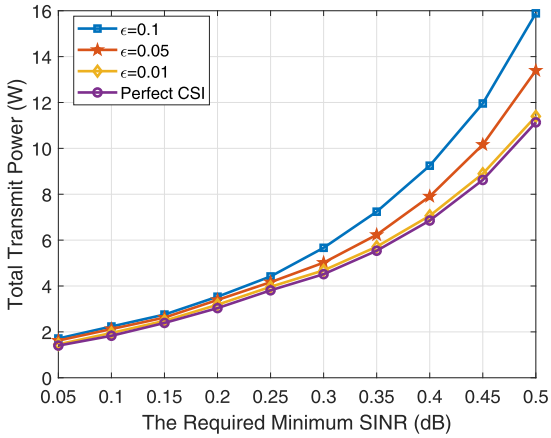

Fig. 10. Impact of channel estimation error bound ϵ on the performance of Algorithm 2.

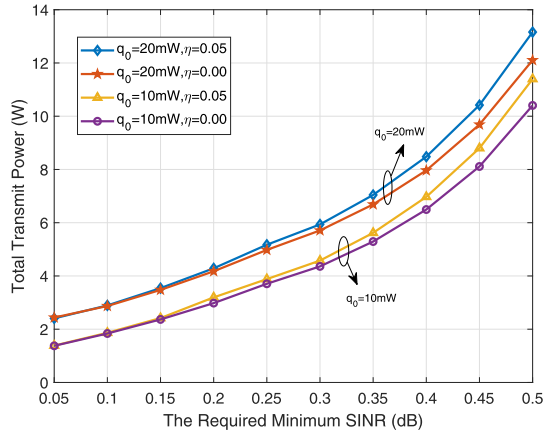

Fig. 11. Influence of imperfect SIC and EH threshold on the performance of Algorithm 2.

always requires more transmit power. This is because there exists a high residual intra-cluster interference after SIC in practical systems. Moreover, the gap between perfect SIC ($\eta = 0.00$) and imperfect SIC is quite small especially at low SINR threshold, which reconfirms that Algorithm 2 has a strong capability of alleviating the impact of imperfect SIC.

V. Conclusion

In this paper, we exploit the benefits of a multiple-antenna BS for supporting massive SWIPT in the cellular IoT. In particular, we propose two robust beamforming algorithms for maximizing the weighted sum rate and minimizing the total power consumption, respectively. Extensive simulation results demonstrated that the proposed algorithms are efficient to alleviate the impacts of practically adverse factors, e.g., imperfect SIC, non-linear EH, channel uncertainty, and limited radio spectrum, and thus enhance their applications in the cellular IoT.

Massive access in the NOMA-based cellular IoT with SWIPT has not been well addressed, and it will continue to be a critical issue in the next-generation cellular IoT networks. In the following, we list two research directions in future works. First, channel estimation is a critical issue for performance enhancement by interference coordination in cellular IoT. Hence, it makes sense to design an efficient channel estimation method for cellular massive IoT. Second, a practical bottleneck of wireless power transfer is the low efficiency due to path loss. In other words, the UEs far from the BS harvest a small amount of energy, resulting in narrow coverage. In addition to the use of a large-scale antenna array at the BS, it is possible to introduce new techniques into cellular massive IoT with SWIPT to expand the coverage, such as large intelligent surface.

Appendix A
The Proof of Theorem 1

For convenience of expression, let $\{\mathbf{W}_m^{(t)}, x_{m,n}^{(t)}, y_{m,n}^{(t)}, t = 1, 2, \cdots\}$ be the solutions of problem (32) in the tth iteration. Before performing iteration, we first set a feasible initial value $\mathbf{w}_m^{(0)}$. Based on the initial value $\mathbf{W}_m^{(0)} = \mathbf{w}_m^{(0)}(\mathbf{w}_m^{(0)})^H$, we can get $\tilde{y}_{m,n}^{(1)}$. Then, the solutions of the first round of iteration $\{\mathbf{W}_m^{(1)}, x_{m,n}^{(1)}, y_{m,n}^{(1)}\}$ can be obtained accordingly. Finally, we need to ensure the feasibility of the initial value base on the constraint that $x_{m,n}$ and $y_{m,n}$ are positive. Due to the form of the objective function (32a), the optimal solution $y_{m,n}^{(t)}$ is required to satisfy

$$y_{m,n}^{(t)} \le \tilde{y}_{m,n}^{(t)}. \tag{51}$$

Then, according to the Eq. (31), we have

$$\begin{aligned} e^{\tilde{y}_{m,n}^{(t+1)}} &= e^{\tilde{y}_{m,n}^{(t)}} \left(y_{m,n}^{(t)} - \tilde{y}_{m,n}^{(t)} + 1 \right) \\ &\le e^{y_{m,n}^{(t)}}, \end{aligned} \tag{52}$$

where $e^{\tilde{y}_{m,n}^{(t+1)}} = \sum_{j=1}^{M} \sum_{i=1}^{N_j} \varphi_{j,i}^{m,n} \alpha_{j,i} (\hat{\mathbf{h}}_{m,n}^H \mathbf{W}_j^{(t)} \hat{\mathbf{h}}_{m,n} + 2\epsilon_{m,n} \|\mathbf{W}_j^{(t)} \hat{\mathbf{h}}_{m,n}\|) + \sigma_0^2 + \frac{\sigma_1^2}{\rho_{m,n}}$. Combine (51) and (52), it is obtained that

$$\tilde{y}_{m,n}^{(t+1)} \le y_{m,n}^{(t)} \le \tilde{y}_{m,n}^{(t)}, \tag{53}$$

i.e., $\{\tilde{y}_{m,n}^{(t)}\}$ is monotonically decreasing. Moreover, as mentioned in (27), we have $e^{\tilde{y}_{m,n}^{(t)}} \ge e^{y_{m,n}^{(t)}} \ge \sigma_0^2 + \frac{\sigma_1^2}{\rho_{m,n}}$, which means $\{\tilde{y}_{m,n}^{(t)}\}$ has a lower bound. According to the monotone convergence theorem, sequence $\{\tilde{y}_{m,n}^{(t)}\}$ would converge. Once $\{\tilde{y}_{m,n}^{(t)}\}$ converges, the solution $\{y_{m,n}^{(t)}\}$ would also converge due to Eq. (51). Because of $y_{m,n}^{(t+1)} \le y_{m,n}^{(t)}$, the solutions $\{x_{m,n}^{(t)}, y_{m,n}^{(t)}\}$ obtained in the tth iteration are feasible in the $(t+1)$th iteration. Then, due to the form of the objective function (32a), we have

$$x_{m,n}^{(t+1)} \ge x_{m,n}^{(t)}, \tag{54}$$

which means $\{x_{m,n}^{(t)}\}$ is monotonically increasing. Since $\mathbf{W}_m$ is limited by $P_{\max}$, $x_{m,n}^{(t)}$ is bounded, i.e., $\{x_{m,n}^{(t)}\}$ has an upper bound. Based on the monotone convergence theorem, sequence $\{x_{m,n}^{(t)}\}$ would converge. Thus, the solutions $\{x_{m,n}^{(t)}, y_{m,n}^{(t)}, t = 1, 2, \ldots\}$ generated by the proposed Algorithm 1 would converge. As a result, the optimal solution $\{\mathbf{W}_m^{(t)}\}$ to problem (32) would converge in the iterations.

REFERENCES

[1] Q. Qi, X. Chen, D. W. K. Ng, C. Zhong, and Z. Zhang, "Robust beamforming design for SWIPT in cellular internet of things," in *Proc. IEEE/CIC Int. Conf. Commun.*, Changchun, China, Aug. 2019, pp. 523–528.

[2] M. R. Palattella *et al.*, "Internet of things in the 5 G era: Enablers, architecture, and business models," *IEEE J. Sel. Areas Commun.*, vol. 34, no. 3, pp. 510–527, Mar. 2016.

[3] "Technical specification group GSM/EDGE radio access network; Cellular system support for ultra-low complexity and low throughput internet of things (CIoT)," 3GPP, Sophia Antipolis Cedex, France, TR 45.820, Nov. 2015.

[4] A. Zanella, N. Bui, A. Castellani, L. Vangelista, and M. Zorzi, "Internet of things for smart cities," *IEEE Internet Things J.*, vol. 1, no. 1, pp. 22–32, Feb. 2014.

[5] L. D. Xu, W. He, and S. Li, "Internet of Things in industries: A survey," *IEEE Trans. Ind. Informat.*, vol. 10, no. 4, pp. 2233–2243, Nov. 2014.

[6] M. Shirvnimoghaddam, M. Condoluci, M. Dohler, and S. J. Johnson, "On the fundamental limits of random non-orthogonal multiple access in cellular massive IoT," *IEEE J. Sel. Areas Commun.*, vol. 35, no. 10, pp. 2238–2252, Oct. 2017.

[7] Z. Chen, Z. Ding, X. Dai, and G. K. Karagiannidis, "On the application of quasi-degradation to MISO-NOMA downlink," *IEEE Trans. Signal Process.*, vol. 64, no. 23, pp. 6174–6189, Dec. 2016.

[8] L. Dai, B. Wang, Y. Yuan, S. Han, C. L. I, and Z. Wang, "Non-orthogonal multiple access for 5 G: Solutions, challenges, opportunities, and future research trends," *IEEE Commun. Mag.*, vol. 53, no. 9, pp. 74–81, Sep. 2015.

[9] X. Chen, *Massive Access for Cellular Internet of Things Theory and Technique*, Berlin, Germany: Springer, 2019.

[10] Z. Ding, X. Lei, G. K. Karagiannidis, R. Schober, J. Yuan, and V. K. Bhargava, "A survey on non-orthogonal multiple access for 5 G networks: Research challenges and future trends," *IEEE J. Sel. Areas Commun.*, vol. 35, no. 10, pp. 2181–2195, Oct. 2017.

[11] A. Agrawal, J. G. Andrews, J. M. Cioffi, and T. Meng, "Iterative power control for imperfect successive interference cancellation," *IEEE Trans. Wireless Commun.*, vol. 4, no. 3, pp. 878–884, Mar. 2005.

[12] S. M. R. Islam, N. Avazov, O. A. Dobre, and K-S. Kwak, "Power-domain non-orthogonal multiple access (NOMA) in 5 G: Potentials and challenges," *IEEE Commun. Surv. Tut.*, vol. 19, no. 2, pp. 721–742, Jun. 2017.

[13] X. Chen, Z. Zhang, C. Zhong, R. Jia, and D. W. K. Ng, "Fully non-orthogonal communication for massive access," *IEEE Trans. Commun.*, vol. 66, no. 4, pp. 1717–1731, Apr. 2018.

[14] H. Sun, B. Xie, R. Q. Hu, and G. Wu, "Non-orthogonal multiple access with SIC error propagation in downlink wireless MIMO networks," in *Proc. IEEE 84th Veh. Technol. Conf.*, Sep. 2016, pp. 1–5.

[15] M. F. Hanif, Z. Ding, T. Ratnarajah, and G. K. Karagiannidis, "A minorization-maximization method for optimizing sum rate in the downlink of non-orthogonal multiple access systems," *IEEE Trans. Signal Process.*, vol. 64, no. 1, pp. 76–88, Jan. 2016.

[16] X. Chen, Z. Zhang, C. Zhong, and D. W. K. Ng, "Exploiting multiple-antenna for non-orthogonal multiple access," *IEEE J. Sel. Areas Commun.*, vol. 35, no. 10, pp. 2207–2220, Oct. 2017.

[17] F. Alavi, K. Cumanan, Z. Ding, and A. G. Burr, "Robust beamforming techniques for non-orthogonal multiple access systems with bounded channel uncertainties," *IEEE Commun. Lett.*, vol. 21, no. 9, pp. 2033–2036, Sep. 2017.

[18] F. Alavi, K. Cumanan, Z. Ding, and A. G. Burr, "Beamforming techniques for non-orthogonal multiple access in 5 G cellular networks," *IEEE Trans. Veh. Technol.*, vol. 67, no. 10, pp. 9474–9487, Oct. 2018.

[19] W. Na, J. Park, C. Lee, K. Park, J. Kim, and S. Cho, "Energy-efficient mobile charging for wireless power transfer in internet of things networks," *IEEE Internet Things J.*, vol. 5, no. 1, pp. 79–92, Jan. 2018.

[20] Q. Qi and X. Chen, "Wireless powered massive access for cellular internet of things with imperfect SIC and nonlinear EH," *IEEE Internet Things J.*, vol. 6, no. 2, pp. 3110–3120, Apr. 2019.

[21] X. Chen, C. Yuen, and Z. Zhang, "Wireless energy and information transfer tradeoff for limited feedback multi-antenna systems with energy beamforming," *IEEE Trans. Veh. Technol.*, vol. 63, no. 1, pp. 407–412, Jan. 2014.

[22] X. Chen, Z. Zhang, H-H. Chen, and H. Zhang, "Enhancing wireless information and power transfer by exploiting multi-antenna techniques," *IEEE Commun. Mag.*, vol. 53, no. 4, pp. 133–141, Apr. 2015.

[23] E. Boshkovska, A. Koelpin, D. W. K. Ng, N. Zlatanov, and R. Schober, "Robust beamforming for SWIPT systems with non-linear energy harvesting model," in *Proc. IEEE 17th Int. Workshop Signal Process. Advances Wireless Commun.*, 2016, pp. 1–5.

[24] J. Xue *et al.*, "Transceiver design of optimum wirelessly powered full-duplex MIMO IoT devices," *IEEE Trans. Commun.*, vol. 66, no. 5, pp. 1955–1969, May 2018.

[25] M. F. Hanif, L. Tran, A. Tolli, M. Juntti, and S. Glisic, "Efficient solutions for weighted sum rate maximization in multicellular networks with channel uncertainties," *IEEE Trans. Signal Process.*, vol. 61, no. 22, pp. 5659–5674, Nov. 2013.

[26] Y. Xu *et al.*, "Joint beamforming and power-splitting control in downlink cooperative SWIPT NOMA systems," *IEEE Trans. Signal Process.*, vol. 65, no. 18, pp. 4874–4886, Sep. 2017.

[27] H. Sun, F. Zhou, R. Q. Hu, and L. Hanzo, "Robust beamforming design in a NOMA cognitive radio network relying on SWIPT," *IEEE J. Sel. Areas Commun.*, vol. 37, no. 1, pp. 142–155, Jan. 2019.

[28] I. Krikidis, S. Timotheou, S. Nikolaou, G. Zheng, D. W. K. Ng, and R. Schober, "Simultaneous wireless information and power transfer in modern communication systems," *IEEE Commun. Mag.*, vol. 52, no. 11, pp. 104–110, Nov. 2014.

[29] D. W. K. Ng, E. S. Lo, and R. Schober, "Wireless information and power transfer: Energy efficiency optimization in OFDMA systems," *IEEE Trans. Wireless Commun.*, vol. 12, no. 12, pp. 6352–6370, Dec. 2013.

[30] X. Chen, X. Wang, and X. Chen, "Energy-efficient optimization for wireless information and power transfer in large-scale MIMO systems employing energy beamforming," *IEEE Wireless Commun. Lett.*, vol. 2, no. 6, pp. 667–670, Dec. 2013.

[31] T. Le, K. Mayaram, and T. Fiez, "Efficient far-field radio frequency energy harvesting for passively powered sensor networks," *IEEE J. Solid-State Circuits*, vol. 43, no. 5, pp. 1287–1302, May 2008.

[32] J. Guo and X. Zhu, "An improved analytical model for RF-DC conversion efficiency in microwave rectifiers," in *Proc. IEEE MTT-S Int. Microw. Symp. Dig.*, Jun. 2012, pp. 1–3.

[33] Q. Li and W. Ma, "Spatially selective artificial-noise aided transmit optimization for MISO multi-eves secrecy rate maximization," *IEEE Trans. Signal Process.*, vol. 61, no. 10, pp. 2704–2717, May 2013.

[34] G. H. Hardy, J. E. Littlewood, and G. Polya, *Inequalities*. Cambridge, U.K.: Cambridge Univ. Press, 1952.

[35] S. Boyd and L. Vandenberghe, *Convex Optimization*. Cambridge, U.K.: Cambridge Univ. Press, 2004.

[36] M. Grant and S. Boyd, "CVX: MATLAB software for disciplined convex programming," [Online]. Available: http://cvxr.com/cvx. Accessed on: Sep. 2013.

[37] G. Pataki, "On the rank of extreme matrices in semidefinite programs and the multiplicity of optimal eigenvalues," *Math. Oper. Res.*, vol. 23, pp. 339–358, May 1998.

[38] A. Ben-Tal and A. Nemirovski, *Lectures on Modern Convex Optimization: Analysis, Algorithms, and Engineering Applications* (MPS-SIAM Series on Optimization). Philadelphia, PA, USA: SIAM, 2001.

[39] Y. Huang, D. Palomar, and S. Zhang, "Lorentz-positive maps and quadratic matrix inequalities with applications to robust MISO transmit beamforming," *IEEE Trans. Signal Process.*, vol. 61, no. 5, pp. 1121–1130, Mar. 2013.

[40] S. Krishnamurthy and R. Tzoneva, "Investigation on the impact of the penalty factors over solution of the dispatch optimization problem," in *Proc. IEEE Int. Conf. Ind. Technol.*, 2013, pp. 851–860.

Qiao Qi (S'19) received the B.S. degree in communication engineering from Hangzhou Dianzi University, Hangzhou, China, in 2018. She is currently working toward the M.S. degree with the College of Information Science and Electronic Engineering, Zhejiang University, Hangzhou, China. Her research interests include massive access, wireless power transfer, and cellular IoT.

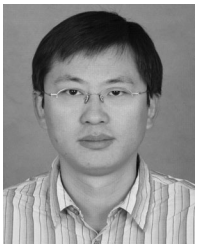

Xiaoming Chen (M'10–SM'14) received the B.Sc. degree from Hohai University, Nanjing, China, in 2005, the M.Sc. degree from the Nanjing University of Science and Technology, Nanjing, China, in 2007, and the Ph.D. degree from Zhejiang University, Hangzhou, China, in 2011, all in electronic engineering. He is currently a Professor with the College of Information Science and Electronic Engineering, Zhejiang University, Hangzhou, China. From March 2011 to October 2016, he was with Nanjing University of Aeronautics and Astronautics, Nanjing, China. From February 2015 to June 2016, he was a Humboldt Research Fellow with the Institute for Digital Communications, Friedrich-Alexander-University Erlangen-Nürnberg (FAU), Germany. His research interests mainly focus on massive access, Internet of Things, and smart communications.

Dr. Chen was an Editor for the IEEE COMMUNICATIONS LETTERS, and currently an Editor for the IEEE TRANSACTIONS ON COMMUNICATIONS and a Lead Guest Editor of IEEE JSAC Massive Access for 5G and Beyond. He was an Exemplary Reviewer for the IEEE COMMUNICATIONS LETTERS in 2014, and IEEE TRANSACTIONS ON COMMUNICATIONS from 2015 to 2018. He was a recipient of Best Paper Awards of IEEE ICC 2019 and IEEE/CIC ICCC 2018.

Derrick Wing Kwan Ng (S'06–M'12–SM'17) received the bachelor's (Hons.) and M.Phil. degrees in electronic engineering from the Hong Kong University of Science and Technology (HKUST), Hong Kong, in 2006 and 2008, respectively, and the Ph.D. degree from The University of British Columbia (UBC), Vancouver, BC, Canada, in 2012. He was a Senior Postdoctoral Fellow with the Institute for Digital Communications, Friedrich-Alexander-University Erlangen-Nürnberg (FAU), Germany. He is currently a Senior Lecturer and an ARC DECRA Research Fellow with the University of New South Wales, Sydney, NSW, Australia. His research interests include convex and non-convex optimization, physical layer security, wireless information and power transfer, and green (energy-efficient) wireless communications.

Dr. Ng was the recipient of the Best Paper Awards at the IEEE TCGCC Best Journal Paper Award 2018, INISCOM 2018, IEEE International Conference on Communications (ICC) 2018, IEEE International Conference on Computing, Networking and Communications (ICNC) 2016, IEEE Wireless Communications and Networking Conference (WCNC) 2012, the IEEE Global Telecommunication Conference (Globecom) 2011, and the IEEE Third International Conference on Communications and Networking in China 2008. He is currently an Area Editor for the IEEE Open Journal of the Communications Society, an Editor for the IEEE TRANSACTIONS ON WIRELESS COMMUNICATIONS, IEEE TRANSACTIONS ON GREEN COMMUNICATIONS AND NETWORKING, IEEE OPEN JOURNAL OF VEHICULAR TECHNOLOGY, and a Guest Editor of IEEE JSAC Multiple Antenna Technologies for Beyond 5G, IEEE JSAC Massive Access for 5G and beyond. Besides, he has been serving as an Editorial Assistant to the Editor-in-Chief for the IEEE TRANSACTIONS ON COMMUNICATIONS since January 2012. In addition, he is listed as a Highly Cited Researcher by Clarivate Analytics in 2018 and 2019.